

Deciphering the Chemical Bonding in Anionic Thallium Clusters

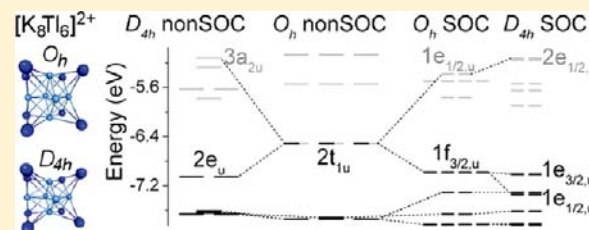
Fei Wang,[†] Ulrich Wedig,[†] Dasari L. V. K. Prasad,^{†,‡} and Martin Jansen^{*,†}

[†]Max Planck Institute for Solid State Research, Heisenbergstrasse 1, 70569 Stuttgart, Germany

[‡]Department of Chemistry and Chemical Biology, Cornell University, Ithaca, New York 14853, United States

S Supporting Information

ABSTRACT: The chemical bonding schemes of thallium cluster anions commonly comply with neither Wade–Mingos’s rules nor the Zintl–Klemm concept and thus far have escaped a fully consistent description. In general, the number of electrons available for the cluster skeleton bonding fall below those required according to the qualitative concepts mentioned and the clusters were labeled “hypoelectronic”. Based on fully relativistic band structure calculations on respective complete extended solids and electronic structure calculations on excised, charge compensated, and geometrically optimized clusters, we have identified two mechanisms that are suited to lift the degeneracy of partially filled electronic states and to open a HOMO–LUMO gap, the Jahn–Teller effect and relativistic spin–orbit coupling. Treatment on this level of theory shows that, in accordance with experiment, the thallium cluster anions known are electronically saturated and not deficient in valence electrons. We provide qualitative group theoretical procedures for analyzing the Jahn–Teller effect and spin–orbit coupling in lifting the degeneracy of frontier orbitals in highly symmetric thallium cluster anions.



INTRODUCTION

A stable chemical configuration corresponds to a locally ergodic region on the energy landscape of chemical matter¹ and features, at the given boundary conditions, a specific equilibrium structure, a distinct electronic ground state, and a characteristic set of properties. All these attributes, in principle, can be revealed experimentally, or computationally by solving Schrödinger’s equation. However, quantitative numerical descriptions as achieved by calculations usually provide huge arrays of continuously varying data. Thus, such approaches, although delivering physically correct descriptions, generate results that are hardly comprehensible by human brain and do not furnish “understanding”.² However, a “conceptual comprehension” is a necessary prerequisite for communicating and teaching science, and moreover, for developing creativity in research planning. For these reasons, the results of quantitative calculations used to be, and still need to be, cast in “concepts”.³ Although one has to pay the price of, e.g., loss of information, deformation of the reality, squeezing continuous variations into rigid and far too coarse grids, or partitioning properties, which are intrinsically continuous, into discrete increments, such strategy has a long tradition in chemistry and its virtue is beyond question.

Probably the most widely used conceptual approaches are aiming at classifying the chemical bond by type and strength. The latter hierarchical point of view is particularly well suited to partition extended solids. For crystalline solids consisting of molecules, where the intra- and intermolecular bonds are easily discernible by length and strength, this is obviously a beneficial procedure.

This way of analyzing solids is losing stringency, however, with the bonds approaching balance until equivalence. Among








the tremendous diverseness of combinations encountered in chemistry, solid materials featuring well-distinguishable homoatomic substructures, i.e., clusters, which can be excised from the extended crystal structures by imagination or in reality, have attracted a lot of interest. For such cluster compounds a rather efficient set of qualitative tools for classification and stability assessing has become available. The Zintl–Klemm^{4–6} concept and Wade’s rules (extended by Mingos)^{7–9} are among the most prominent ones. Their great popularity is based on simplicity and quite general validity. In a sense, the Zintl–Klemm concept and Wade’s rules are complementary, as can be seen when inspecting clusters from the third group elements. Wade’s rules give an excellent account of the systematics of boranes, while the Zintl–Klemm concept appears to be superior when analyzing, e.g., aluminides. Against the background of the success of the available cluster concepts, it is quite puzzling to see them fail in the special case of thallium clusters, and it comes as a kind of historical irony that Zintl’s initial touchstone at developing his concept was the 3D-infinite $[\text{Tl}^-]_n$ network in NaTl.^{4,10}

Corbett and co-workers have explored and documented to a large extent the meanwhile rather extended and manifold class of Tl clusters.¹¹ It is extraordinary that most of them do not have sufficient skeletal electrons as required by the Wade–Mingos rules (at least $2n+2$ skeletal electrons for a Tl_n cluster). They have thus been classified as “hypoelectronic” considering the thallium 6s orbitals as “inert”, i.e., not contributing to the cluster bonding. This effect is basically related to the scalar relativistic stabilization of the s-orbitals of heavy elements.¹²

Received: October 5, 2012

Published: November 14, 2012

Table 1. Survey of Homoatomic Tl Clusters

Cluster	Structure ^a	Symmetry	Compound	Magnetism	Resistivity ($\mu\Omega\cdot\text{cm}$)	Ref.	Formal Charge	Skeletal Electrons
Tl ₄		C_2	Na ₂ Tl	-	-	26	-8	12 ($2n + 4$)
		$C_s(\sim C_{3v})$	Na ₂₃ K ₁₉ Tl _{15,33}	<i>para</i>	~90 (293K)	27		
Tl ₅		$C_s(\sim D_{3h})$	Na ₂ K ₂₁ Tl ₁₉	<i>dia</i>	~200 (243K)	13	-7	12 ($2n + 2$)
		D_{3h}	Na ₂₃ K ₁₉ Tl _{15,33}			27		
Tl ₆		O_h	Na ₁₄ K ₆ Tl ₁₈ M ^b	<i>para</i>	~100 (290K)	28	-8	14 ($2n + 2$)
		$D_{3d}(\sim O_h)$	Cs ₄ Tl ₂ O	<i>dia</i>	-	19	-6	12 ($2n$)
		$C_{2h}(\sim D_{4h})$	KTl	<i>dia</i>	-	14		
		$D_2(\sim D_{4h})$	CsTl	<i>dia</i>	~10 ⁶ (293K)	15	-6	12 ($2n$)
		$C_{2v}(\sim D_{4h})$	A ₁₀ Tl ₆ O ₂ ^c	-	-	16		
Tl ₇		$C_1(\sim D_{5h})$	K ₁₀ Tl ₇	<i>para</i>	-	17	-7	14 ($2n$)
		$C_{2v}(\sim D_{5h})$	Na ₁₂ K ₃₈ Tl ₄₈ Au ₂	<i>para</i>	~765 (298K)	18		
Tl ₈		T_d	Cs ₁₈ Tl ₈ O ₆	<i>dia</i>	-	20	-6	14 ($2n - 2$)
		D_{3d}	Cs ₈ Tl ₈ O	<i>dia</i>	-	25		
Tl ₉		C_{2v}	Na ₂ K ₂₁ Tl ₁₉ Na ₁₂ K ₃₈ Tl ₄₈ Au ₂			13 18	-9	18 ($2n - 2$)
		$D_3(\sim D_{3h})$	A ₈ Tl ₁₁ ^c	<i>para</i>	~231 (298K, A = K)	29		
Tl ₁₁		D_{3h}	A ₁₅ Tl ₂₇ ^c	<i>para</i>	~34 (293K, A = Rb)	30	-7	18 ($2n - 4$)
		$C_{3v}(\sim D_{3h})$	K ₂₁ Tl ₂₂ O ₂	-	-	31		
		C_{3v}	K ₂₁ Tl ₂₂ O ₂	-	-	31	-10	21 ($2n - 1$)

^aTo save space, when clusters from different compounds have similar structures, only one sketch is given. ^bM = Mg, Zn, Cd, Hg. ^cA = alkaline metals.

Some preliminary studies with extended Hückel theory (EHT) calculations have been done; however, there is no systematic investigation yet and neither is there a fully satisfying rationalization given.

One convincing argument, though, is the Jahn–Teller (JT) effect. Respective Tl clusters adopt structures different from the deltahedral shapes required by Wade–Mingos rules. They are lower in symmetry and require less skeletal electrons to fill the bonding molecular orbitals (MOs) and to reach a significant HOMO–LUMO gap resulting in a close-shell electronic configuration. The JT effect can successfully rationalize the structures of “compressed” (D_{4h} and $\sim D_{4h}$) [Tl₆]⁶⁻, [Tl₇]⁷⁻, and [Tl₉]⁹⁻.^{10,13–18} However, this effect does not apply to all of the “hypoelectronic” Tl clusters. Actually, it fails in the case of the almost nondistorted octahedral ($\sim O_h$) [Tl₆]⁶⁻, in Cs₄Tl₂O,¹⁹ which has virtually no JT distortion, and it can neither satisfactorily rationalize the tetrahedral star (T_d) [Tl₈]⁶⁻ in Cs₁₈Tl₈O₆.²⁰ We thus note that there is no consistent model yet that allows us to analyze the chemical bonding in homoatomic Tl clusters. It is, therefore, necessary and beneficial to conduct a systematic investigation into these

“hypoelectronic” Tl clusters to obtain a deeper and more comprehensive understanding of their bonding systematics.

An important factor that has been for long neglected are the nonscalar relativistic effects, especially spin–orbit coupling (SOC), which is not significant for light elements like boron but much more relevant for heavy elements like thallium.^{12,21,22} In this contribution we demonstrate that the apparent peculiarities of the cluster chemistry of thallium can be resolved by considering SOC as a significant factor of influence, in addition to JT distortions, that can lift degeneracy of partially filled frontier orbitals, thus stabilizing particular cluster geometries. Our studies have further revealed that the respective ground state configurations realized benefit to different degrees from either JT or SOC, and in some cases the existence of highly symmetric clusters can only be rationalized on the basis of SOC.

LITERATURE SURVEY OF HOMOATOMIC TL CLUSTERS

A broad spectrum of Tl clusters has been observed in intermetallics and suboxides. From the available comprehensive reviews and more recent literature, all the principle

configurations known for homoatomic Tl clusters were gathered and tabulated in Table 1. In addition, a number of centered and heteroatomic Tl clusters are known.¹¹ Including them would require to consider qualitatively different aspects of cluster bonding, which is beyond the scope of this present study.

All the clusters compiled in Table 1 are isolated. No covalent exobonds like the B–H bonds in boranes or intercluster bonds in, e.g., Rb_2In_3 ^{23,24} are present. Even in the suboxides, the clusters are exclusively surrounded by electropositive elements. Assuming complete charge transfer according to the Zintl–Klemm concept, highly negative formal cluster charges result. Besides the charges, another formal descriptor characterizing the clusters, the number of skeletal electrons contributing to the intracluster bonds, is listed in Table 1. This number is the sum of the thallium 6p electrons, one per atom, plus the absolute value of the formal charge.

Some examples shown in Table 1 document a conspicuous feature of the thallium cluster chemistry. Despite an identical atom number and electron count, clusters may exhibit different shapes. They even may adopt high symmetry, which would, in a conventional point of view, suggest partially filled frontier orbitals, in contrast to the experimental observations. A remarkable representative is the $[\text{Tl}_8]^{6-}$ cluster. It exists with the shape of a parallelepiped (D_{3d}) in $\text{Cs}_8\text{Tl}_8\text{O}^{25}$ and as tetrahedral star (T_d) in $\text{Cs}_{18}\text{Tl}_8\text{O}_6$.²⁰ The latter cluster is the first thallium cluster, where the relevance of SOC at lifting the degeneracy of the cluster HOMO was demonstrated.²⁰ Another example¹⁹ is $[\text{Tl}_6]^{6-}$, which exists both as a regular and as a highly JT distorted octahedron. This cluster will serve as a prototype in the further discussion.

Summing up, in analyzing the bonding characteristics of homoatomic thallium clusters, it is indispensable to consider (a) the interplay or competition of the JT effect and SOC in achieving closed-shell electronic configurations and (b) the interaction of itinerant electrons with the cluster orbitals in metallic systems.

In the next section we present the computational methods involved in deciphering the chemical bonding in the thallium clusters studied here. Each cluster specified in Table 1 is embedded in a crystalline compound, thus the “correct” description of the respective electronic structure requires periodic band structure calculations. Yet, it is far from trivial to extract a meaningful cluster MO picture from the resulting data. However, comparing cluster calculations and periodic ones will facilitate the analysis of the various aspects of cluster bonding.²⁰

COMPUTATIONAL METHODS

All the calculations on clusters and solids were performed with and without periodic boundary conditions, respectively, in the framework of density functional theory (DFT), applying the GGA-functional (generalized gradient approximation) proposed by Perdew, Becke and Ernzerhof,³² in order to ensure a comparable description of exchange and correlation with the various approaches. Spin-polarized systems were computed with the unrestricted Kohn–Sham (UKS) formalisms, i.e., solving separate Kohn–Sham equations for α - and β -spin. In this section, only a general overview of the computational parameters is given. Further details like k -point meshes, cutoffs, atomic radii, and so forth for specific systems and calculations can be found in the Supporting Information.

Band structures and properties of the crystalline systems, based on the respective experimental structure, are computed with either or both of the two program packages, WIEN2k³³ and VASP.³⁴ The two

codes differ in the approach of augmenting the plane-wave basis set. With WIEN2k, in general, the augmented-plane-wave plus local orbital (APW+lo) basis^{35,36} was used. VASP calculations were based on the projector augmented-wave (PAW) method.^{37,38} With these augmentations, both codes yield all-electron band structures and densities in a scalar relativistic approximation.³⁹ SOC can be included in WIEN2k by a second variational method.⁴⁰ In VASP the implementation is based on the code for the description of noncollinear magnetic structures.⁴¹ In the latter case, use of symmetry was switched off.

Cluster calculations for specific configurations, minimum searches and scans through the energy landscape were performed with the TURBOMOLE program package.⁴² Due to the high negative charge of the naked Tl clusters, they were embedded in a shell of alkaline atoms, capping the faces of the polyhedron (for example, as shown in Figure 7). The overall charge of this arrangement was chosen to mimic a certain formal charge, i.e., $[\text{K}_8\text{Tl}_6]^{2+}$ or $[\text{Cs}_8\text{Tl}_6]^{2+}$ for $[\text{Tl}_6]^{6-}$ or Cs_8Tl_6 for $[\text{Tl}_6]^{8-}$.

Scalar relativistic contributions were included in the cluster calculations with the standard RI-DFT⁴³ code by choosing appropriate pseudopotentials, leaving 21 electrons for Tl^{44} and 9 electrons for Cs^{45} in the valence shell. The def2-TZVP basis set⁴⁶ was used. For relativistic calculations including SOC, the two-component formalism as implemented in TURBOMOLE⁴⁷ was applied. In this case, the spin–orbit terms⁴⁴ had to be added to the thallium pseudopotential, and the modified def2-TZVP-2c basis set⁴⁸ was used. With the present implementation, no spacial symmetry operations could be exploited. The existence of local minima in the energy landscape was verified by the analysis of the Hessian matrix. In the case of the two-component formalism, the Hessian matrix had to be determined by numerical differentiation (script NumForce).

As the two-component Hamiltonian includes the 2×2 Pauli matrices, the resulting one-particle functions are two-component, complex spinors (eq 1)

$$\phi_k(\mathbf{x}) = \text{Re} \begin{pmatrix} \phi_k^\alpha(\mathbf{r}) \\ \phi_k^\beta(\mathbf{r}) \end{pmatrix} + i \text{Im} \begin{pmatrix} \phi_k^\alpha(\mathbf{r}) \\ \phi_k^\beta(\mathbf{r}) \end{pmatrix} \quad (1)$$

In contrast to the orbitals obtained in a non- or scalar relativistic treatment, spin and orbital momenta are coupled with these spinors, and spin is no longer an observable. However, in order to characterize the clusters in terms of closed- or open-shell systems, the number of unpaired electrons (N_S) can be determined according to eq 2

$$N_S = 2\sqrt{\langle S_x \rangle^2 + \langle S_y \rangle^2 + \langle S_z \rangle^2} \quad (2)$$

S_x , S_y , and S_z are the spin components in the direction of the respective Cartesian axis. N_S is always an integer in scalar relativistic calculations, it may take any positive real value when SOC is considered.

Besides the above-mentioned quantum mechanical program systems, a set of further programs were used. With Critic,⁴⁹ topological analyses of the WIEN2k densities were performed, in order to obtain effective charges of the atoms. Isosurfaces of orbitals or electron densities were either plotted with XCrySDen⁵⁰ or with VESTA.⁵¹

DOUBLE GROUP APPROACH

In non- or scalar relativistic quantum chemistry, generally spin-free Hamiltonians are used. The symmetry of the resulting one-particle eigenfunctions, the orbitals, corresponds to the irreducible representations (irrep) of the point group of the molecule or of the space group of the crystal, respectively. The spin-free treatment yields only half of the states in the eigenvalue spectrum, called the “duplexity phenomena” by Dirac.⁵² This dilemma can be overcome by allowing double occupancy of the orbitals, thus counting them twice.

The full spectrum is obtained by using a Lorentz invariant Hamiltonian or by including Pauli spin matrices, thereby considering SOC. The resulting, singly occupied eigenfunctions

Table 2. Character Table of O_h (Bold) and Its Double Group O_h^*

O_h^*	E	$3C_2, 3QC_2$	$8C_3$	$6C_4$	$6C_2', 6QC_2'$	i	$3\sigma, 3Q\sigma$	$8S_6$	$6S_4$	$6\sigma_d, 6Q\sigma_d$	Q	$8QC_3$	$6QC_4$	Q_i	$8QS_6$	$6QS_4$
A_{1g}	1	1	1	1	1	1	1	1	1	1	1	1	1	1	1	1
A_{2g}	1	1	1	-1	-1	1	1	1	-1	-1	1	1	-1	1	1	-1
E_g	2	2	-1	0	0	2	2	-1	0	0	2	-1	0	2	-1	0
T_{1g}	3	-1	0	1	-1	3	-1	0	1	-1	3	0	1	3	0	1
T_{2g}	3	-1	0	-1	1	3	-1	0	-1	1	3	0	-1	3	0	-1
A_{1u}	1	1	1	1	1	-1	-1	-1	-1	-1	1	1	1	-1	-1	-1
A_{2u}	1	1	1	-1	-1	-1	-1	-1	1	1	1	1	-1	-1	-1	1
E_u	2	2	-1	0	0	-2	-2	1	0	0	2	-1	0	-2	1	0
T_{1u}	3	-1	0	1	-1	-3	1	0	-1	1	3	0	1	-3	0	-1
T_{2u}	3	-1	0	-1	1	-3	1	0	1	-1	3	0	-1	-3	0	1
$E_{1/2g}$	2	0	1	$\sqrt{2}$	0	2	0	1	$\sqrt{2}$	0	-2	-1	$-\sqrt{2}$	-2	-1	$-\sqrt{2}$
$E_{5/2g}$	2	0	1	$-\sqrt{2}$	0	2	0	1	$-\sqrt{2}$	0	-2	-1	$\sqrt{2}$	-2	-1	$\sqrt{2}$
$F_{3/2g}$	4	0	-1	0	0	4	0	-1	0	0	-4	1	0	-4	1	0
$E_{1/2u}$	2	0	1	$\sqrt{2}$	0	-2	0	-1	$-\sqrt{2}$	0	-2	-1	$-\sqrt{2}$	2	1	$\sqrt{2}$
$E_{5/2u}$	2	0	1	$-\sqrt{2}$	0	-2	0	-1	$\sqrt{2}$	0	-2	-1	$\sqrt{2}$	2	1	$-\sqrt{2}$
$F_{3/2u}$	4	0	-1	0	0	-4	0	1	0	0	-4	1	0	4	-1	0

are called spinors (cf. Computational Methods). Point groups now are no longer appropriate to describe their symmetry. Spinors have fermionic (spin 1/2) properties, and a rotation about 360° , which is the identity operation in point groups, changes the sign of the spinor. The double group approach is one solution for this problem. A new symmetry element Q (360° rotation) is introduced, which is not the identity. Applying Q twice, i.e., a 720° rotation, results in the new identity element. Considering all products of Q with the elements of the point group leads to the double point group with doubled group order. The irreps of the double point group are either symmetric (vector irreps) or antisymmetric (spinor irreps) with respect to Q . Only the spinor irreps apply to fermionic systems.

Detailed information about double groups can be found in group theory textbooks.^{53,54} Here we review exemplarily the O_h group and the O_h^* double group as they are relevant for the octahedral $[Ti_6]^{6-}$ clusters discussed later. The point group O_h has 48 elements in 10 classes and 10 vector irreps as shown in Table 2 with the bold fonts. When spin is considered, O_h needs to be expanded to its double group O_h^* , which has 96 elements in 16 classes and, besides the 10 vector irreps, 6 spinor irreps ($E_{1/2g}$ to $F_{3/2u}$).⁵⁵ The correlation between vector and spinor irreps can be obtained by taking the direct products between vector irreps and $E_{1/2g}$, the latter of which is the irrep spanned by the elementary spinor (α, β), see Table 3.

Our attention is drawn by the triple degenerate vector irreps, T_{1g} , T_{2g} , T_{1u} and T_{2u} . If they are partially filled in a spin-free

treatment, they may give rise to a JT distortion. The degenerate MOs are then split due to a symmetry reduction. When SOC is considered, e.g., the T_{1u} orbitals with maximally 6-fold occupancy split into two sets of spinors, double degenerate $E_{1/2u}$ and quadruple degenerate $F_{3/2u}$, where each of the spinors can only be singly occupied. This corresponds to a degeneracy breaking analogous to the JT effect and can affect the electronic structure, which is shown later in our discussions about $[Ti_6]^{6-}$ clusters. Similar analyses have been done with octahedral clusters of transitional metal hexafluorides.⁵⁶ Jahn–Teller coupling Hamiltonians for an octahedral environment including SOC terms up to first order were given recently.⁵⁷

RESULTS AND DISCUSSIONS

The Electronic Structure of TI Cluster Compounds.

It is important to keep in mind that treating the TI clusters as excised polyanions is a quite substantial approximation. Instead of being isolated, they are all embedded in extended structures of intermetallics and suboxides. In order to elaborate the interaction with the cationic sublattice and the relation of localized and delocalized electrons, the underlying band structures have to be studied. On the one hand, it is more challenging to extract straightforwardly “conceptual comprehension” from band structures, on the other hand, the calculations are not biased by the polyanion approximation and, moreover, they offer the opportunity for an evaluation of the validity of a pure cluster view.

The densities of states (DOS) of solid compounds containing various thallium clusters (cf. Table 1) are compiled in Figure 1. SOC was considered in all of the underlying calculations, otherwise some cases (e.g., Cs_4Ti_2O ,¹⁹ $Cs_{18}Ti_8O_6$ ²⁰) may result in even qualitatively wrong electronic structures in comparison to the experimental observations. In the graphs shown in Figure 1, the semicore states ($5s, 5p$) of cesium below -8 eV are omitted for clarity. In the suboxides, the part of the DOS that is related to oxygen is accented in light gray. The oxygen anion is surrounded exclusively by cations in these compounds, thus a direct interaction with the thallium cluster anions can be neglected in the further discussion.

At a first glance, all DOS graphs look very similar, showing two distinct regions. In the energy range between -9 and -4 eV, sets of very narrow bands are apparent. They predominantly have thallium $6s$ character. The integral of the DOS in

Table 3. Direct Products between $E_{1/2g}$ and All Vector Irreps

	A_{1g}	=	$E_{1/2g}$
	A_{2g}	=	$E_{5/2g}$
	E_g	=	$F_{3/2g}$
	T_{1g}	=	$E_{1/2g} \oplus F_{3/2g}$
	T_{2g}	=	$E_{5/2g} \oplus F_{3/2g}$
$E_{1/2g} \otimes$	A_{1u}	=	$E_{1/2u}$
	A_{2u}	=	$E_{5/2u}$
	E_u	=	$F_{3/2u}$
	T_{1u}	=	$E_{1/2u} \oplus F_{3/2u}$
	T_{2u}	=	$E_{5/2u} \oplus F_{3/2u}$

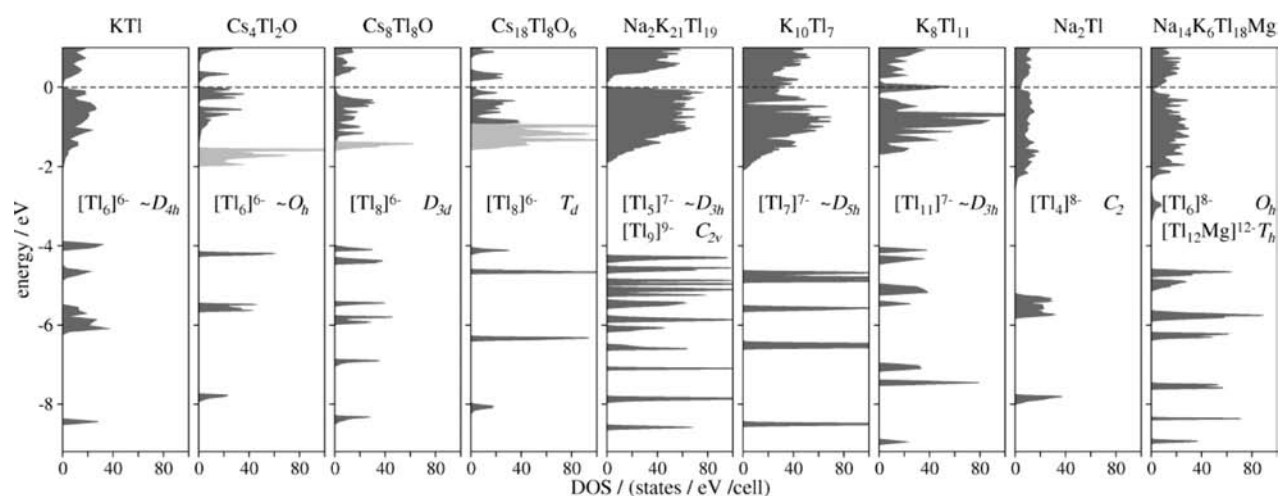


Figure 1. Total densities of states, including SOC, of various thallium cluster compounds. The Fermi energy is shifted to 0 eV respectively. Parts with predominant oxygen character are drawn in light gray.

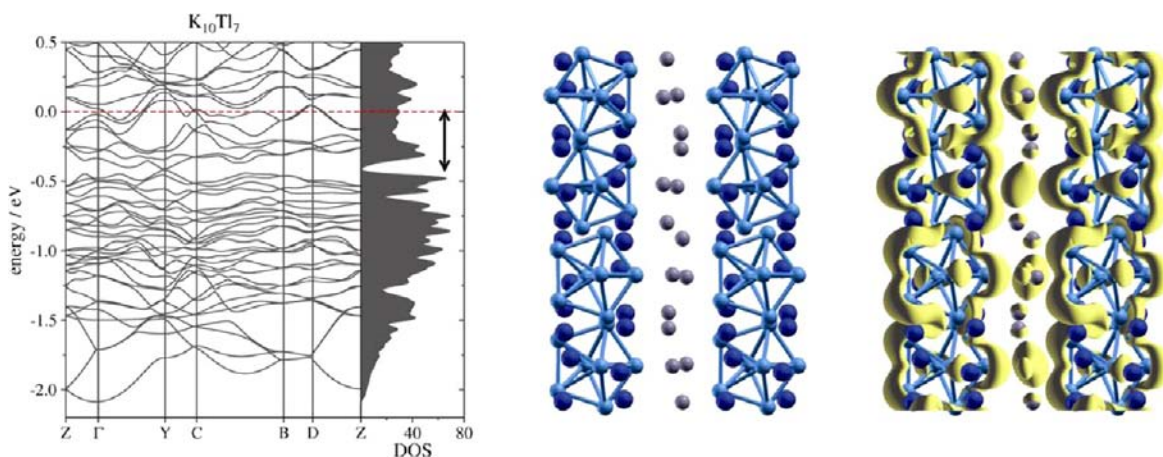


Figure 2. $K_{10}Tl_7$: band structure, DOS and crystal view along [001]. Potassium atoms with high charge are represented by dark blue balls, those with low positive charge by gray balls. The right image includes an isosurface of the electron density ($0.0075 e^-/\text{\AA}^3$) of the bands above the gap at -0.42 eV up to E_F (arrow in the DOS graph).

this region corresponds exactly to the number of 6s atomic orbitals in the clusters. As was shown previously for Cs_8Tl_8O and $Cs_{18}Tl_8O_6$,²⁰ these bands reflect the multiplicity and the position of corresponding lone-pair related cluster MOs. The splitting of these levels on the energy scale will be discussed later in the section dealing with the excised clusters.

The second DOS region of interest is located on the energy scale between -2 eV and the Fermi energy E_F at 0 eV. Neglecting the oxygen contributions in the suboxides, the integrated DOS of these bands with mainly thallium 6p character in all cases amounts to the number of thallium 6p-electrons plus the formal charge rated under the assumption of a complete charge transfer. This sum corresponds to the number of skeletal electrons (cf. Table 1) in those cases where a band gap exists at E_F . This holds true for the first five compounds shown in Figure 1 (KTI , Cs_4Tl_2O , Cs_8Tl_8O , $Cs_{18}Tl_8O_6$ and $Na_2K_{21}Tl_{19}$). The clusters in these compounds are characterized as “hypo-electronic” with $2n$ skeletal electrons in $[Tl_6]^{6-}$ and $[Tl_9]^{9-}$ and $(2n-2)$ skeletal electrons in $[Tl_8]^{6-}$. The only example in this class of semiconducting thallium compounds which fulfills the counting rules for a closo cluster according to Wade–Mingos ($2n+2$) is $[Tl_5]^{7-}$. It is remarkable that this is the only thallium cluster anion where a series of

clusters is known with a pseudo-element relation according to Zintl–Klemm ($[Tl_5]^{7-} - [Sn_5]^{2-}, [Pb_5]^{2-58} - [Bi_5]^{3+59,60}$). It should be mentioned that there also exists such a relation between $[Tl_6]^{6-}$ and the neutral Pb_6 cluster, which recently has been investigated theoretically.⁶¹

In the class of the semiconducting compounds a clear correlation between the formal number of skeletal electrons and the actual electron density distribution exists. This can be demonstrated by comparing the effective charges obtained by a topological analysis of the electron density (so-called Bader charges⁶²). Averaging the effective thallium charges of the various clusters with $2n$ skeletal electrons we obtain a value $-0.64(7) e^-$. The corresponding values for $(2n-2)$ clusters are $-0.48(5)$ and for the $(2n+2)$ cluster $-0.84(3)$. Thus a clear distinction between the different cluster types is possible.

The assignment of a formal number of skeletal electrons as well as their correlation to effective charges is less unambiguous if the compound under discussion is metallic, which is the case for the four compositions on the right side of Figure 1 ($K_{10}Tl_7$, K_8Tl_{11} , Na_2Tl , $Na_{14}K_6Tl_{18}Mg$). An assignment of skeletal electrons can most easily be achieved for K_8Tl_{11} . One itinerant electron per Tl_{11} cluster, represented by the DOS at E_F , is separated by a distinct gap from the region of the DOS which is

related to the skeleton. The specification of a formal charge of 7− for $[\text{Tl}_{11}]^{7-}$ with $(2n - 4)$ skeletal electrons thus appears to be justified.

The situation is more complicated in K_{10}Tl_7 . In the original publication on K_{10}Tl_7 , Kaskel and Corbett¹⁷ assigned a formal charge of 7− to the Tl_7 cluster, based on the bonding and antibonding nature of EHMOs. The three extra electrons per cluster, coming from the cationic sublattice, were regarded as delocalized, inducing the metallic properties of the compound. At first view, the band structure and the density of states (Figure 2) support such an electron count. A gap is noticeable at -0.42 eV, being even more pronounced in the SOC calculations. The integral of the DOS between this gap and the Fermi level (see arrow in Figure 2) amounts to exactly 3 electrons per cluster.

However, is it justified to regard these electrons consistently as itinerant, and do all the cations contribute equally? The topological analysis of the charge density yields a surprising result. The potassium atoms marked by dark blue balls in Figure 2 have an effective Bader charge of $+0.60(1)$. Such a charge is specific for the alkaline atoms in all compounds investigated so far and can be related to a formal charge of +1. In contrast, the potassium atoms marked by gray balls in Figure 2 have a significantly lower positive charge, ranging from $+0.25$ to $+0.46$. The discrimination of the different potassium sites reveals the layered arrangement of the atoms in the crystal.

The layered characteristics of the structure is also reflected by the partial charge density originating from the bands between the gap at -0.42 eV and E_F (Figure 2). Indeed, significant maxima of the charge density are found in the layers formed by the “gray” potassium atoms. But another portion of the charge density surrounds the Tl_7 pentagonal bipyramids, resembling the shape of a diffuse cluster MO. The band structure itself indicates a differentiation of these extra electrons. Flat as well as steep bands are found in the respective energy range. This suggests a description as $[\text{Tl}_7]^{9-}$ plus one extra electron, rather than $[\text{Tl}_7]^{7-}$ plus three extra electrons. The diffuse outer cluster orbital, although antibonding and separated by a gap from the other cluster orbitals, may be considered to be stabilized by the interaction with the itinerant electrons.

The two remaining metallic compounds, Na_2Tl and $\text{Na}_{14}\text{K}_6\text{Tl}_{18}\text{Mg}$, attract attention as they contain, from a formal viewpoint, particular clusters, the so far singular $(2n + 4)$ tetrahedral cluster in Na_2Tl , which is a Wade–Mingos *nido* cluster, and the regular octahedral $[\text{Tl}_6]^{8-}$, a “true” Wade cluster in $\text{Na}_{14}\text{K}_6\text{Tl}_{18}\text{Mg}$. However, in both cases it is difficult to figure out the amount of itinerant electrons and their interaction with the localized cluster MOs. As a further caveat, one needs to keep in mind that syntheses of well-defined single phase samples of these intermetallics are not at all trivial and, in particular, the multicomponent representatives are easily affected by nonstoichiometry and occupational disorder. For Na_2Tl and $\text{Na}_{14}\text{K}_6\text{Tl}_{18}\text{Mg}$ the available experimental data do not appear fully settled and deserve reinvestigation. We therefore have omitted these two candidates from our further considerations.

Assessing the Effects of JT and SOC with the Example of KTI. The JT effect and SOC are independent or joint mechanisms capable of lifting the degeneracy of the frontier orbitals and inducing a closed-shell electronic configuration for the compounds with anionic Tl clusters. In order to elaborate on the nature of these two mechanisms, we compare the electronic structures of the experimental KTI, featuring

“compressed” $[\text{Tl}_6]^{6-}$ octahedral clusters, and a hypothetical polymorphic model structure, containing $[\text{Tl}_6]^{6-}$ clusters with regular O_h symmetry.

The crystal structure of KTI is shown in Figure 3a, which contains $[\text{Tl}_6]^{6-}$ clusters with a “compressed” octahedral

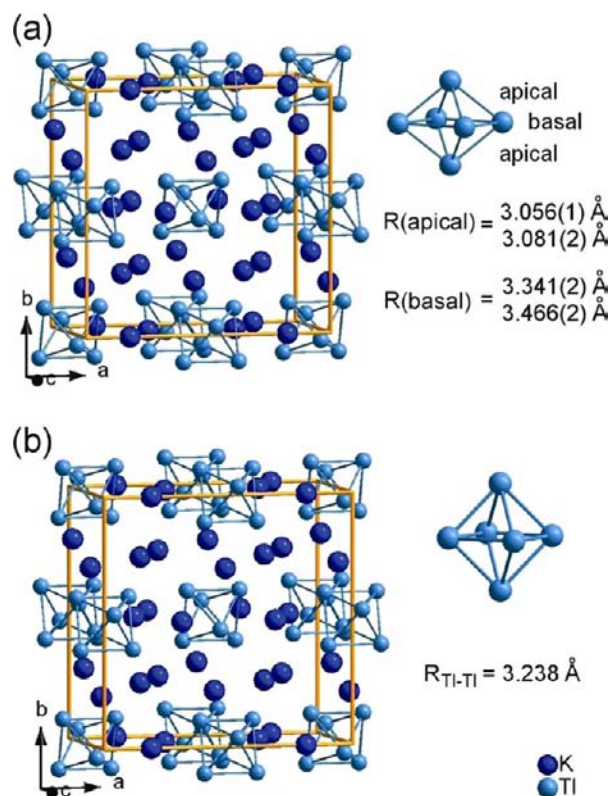


Figure 3. Unit cell and the geometry of the $[\text{Tl}_6]^{6-}$ octahedron in (a) real KTI with C_{2h} $[\text{Tl}_6]^{6-}$ and (b) hypothetical KTI with O_h $[\text{Tl}_6]^{6-}$.

geometry displaying C_{2h} (very close to D_{4h}) instead of O_h symmetry. The formal charge of the cluster is 6−. Out of the 24 valence electrons, 12 are 6s lone pairs and the remaining 12 are 6p electrons providing skeletal bonding. A Wade–Mingos octahedral closo cluster, however, requires $2 \times 6 + 2 = 14$ electrons for skeletal bonding. So the formal $[\text{Tl}_6]^{6-}$ is deficient in electron count by 2 and thus “hypoelectronic”.

Its density of states (DOS) and band structure (non-SOC) are shown in Figure 4. The flat bands located between -9 and -4 eV are related to the inert pairs as discussed before. The states below E_F are contributed dominantly by Tl 6p and K 4s, indicating that K does not donate all valence electrons effectively to Tl, which is in accordance with the Bader’s charge analyses above. However, the PDOS ratio between Tl and K apparently shows that Tl dominates the states below E_F and K dominates those above, implying charge transfer from K to Tl. So KTI has ionic characteristics and treating the $[\text{Tl}_6]^{6-}$ as a polyanion is not stringent but plausible. We also plotted the charge density isosurfaces of the bands below and around E_F . Electrons in these bands are concentrated around the Tl atoms and they reveal apparent skeletal-bonding characteristics within the $[\text{Tl}_6]^{6-}$ clusters.

The band gap at E_F (~ 0.15 eV) manifests that the experimental KTI has the exact number of electrons to achieve a closed-shell configuration, in agreement with the diamagnetism of KTI,¹⁴ and in contradiction with the “hypoelectronicity”

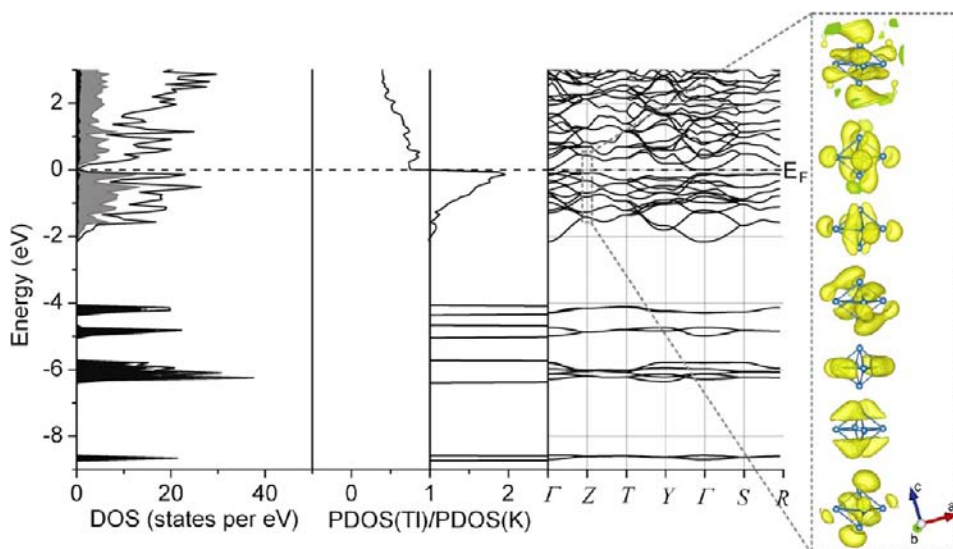


Figure 4. Non-SOC electronic structure of KTI (real structure with C_{2h} $[\text{Tl}_6]^{6-}$): the DOS of KTI (black, Tl s; gray, Tl p; white, K), the ratio between Tl and K PDOS, the band structure of KTI, and the electron density isosurfaces ($\sim 0.001 \text{ e}^-/\text{\AA}^3$) of the selected bands at Z point.

as suggested by Wade–Mingos’s rules. This discrepancy was attributed in previous works^{10,14–16} to the JT effect—in Wade–Mingos’s concept octahedral clusters should have regular O_h symmetry. The symmetry lowering and the associated degeneracy breaking of the partially filled HOMO lends KTI a closed-shell electron configuration. We can confirm this argument here with our hypothetical KTI model structure whose $[\text{Tl}_6]^{6-}$ clusters have O_h symmetry (Figure 3b, more details of this hypothetical model structure are available in the Supporting Information). Its electronic structure is shown in Figure 5. In contrast to the real KTI, E_F does not fall into a gap

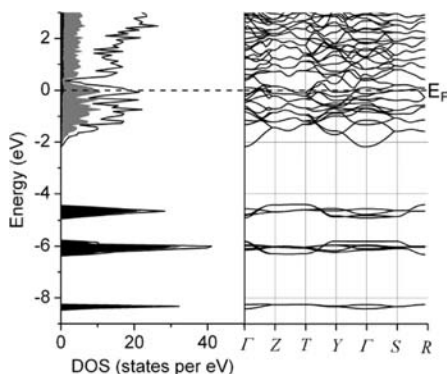


Figure 5. Non-SOC DOS and band structure of the hypothetical KTI with O_h $[\text{Tl}_6]^{6-}$ (black, Tl s; gray, Tl p; white, K).

but crosses a peak of the DOS curve in the hypothetical model structure. However, there is a pseudogap at $\sim 0.4 \text{ eV}$ above E_F . Integrating DOS from E_F to this pseudogap gives 2 electrons per (K_6Tl_6) unit. So KTI with ideal O_h $[\text{Tl}_6]^{6-}$ clusters would have an open-shell configuration and would require 2 more electrons per (K_6Tl_6) unit to reach a virtually closed-shell configuration. This is reminiscent of the 2 electron deficiency of $[\text{Tl}_6]^{6-}$ compared to Wade–Mingos rules. Therefore, the comparison between the real and the hypothetical KTI confirms that the O_h -to- C_{2h} geometric “compression” of the $[\text{Tl}_6]^{6-}$ clusters opens a band gap at E_F , reconciles the electron

deficiency with respect to Wade–Mingos rules, and renders KTI an electron exact closed-shell compound.

However, when applying an analogous JT-based analysis to $\text{Cs}_4\text{Tl}_2\text{O}$,¹⁹ whose Tl clusters are also formally $[\text{Tl}_6]^{6-}$ but have symmetry very close to O_h (D_3 to be precise, and the edge lengths are 3.200(1) and 3.230(2) Å), problems are encountered. Analogous to hypothetical KTI, the electronic structure calculation of $\text{Cs}_4\text{Tl}_2\text{O}$ considering only scalar relativistic effects (just like the calculations above) gives an open-shell electronic configuration. However, magnetometry reveals that $\text{Cs}_4\text{Tl}_2\text{O}$ is diamagnetic,¹⁹ suggesting a closed-shell configuration, which can be rationalized only when the relativistic SOC in Tl is appropriately taken into account (Figure 1). This SOC effect can also be demonstrated here for our hypothetical KTI model structure, whose DOS and band structure are shown in Figure 6a. It is in sharp contrast with the non-SOC result in Figure 5. Apparently, due to the relativistic SOC effect, the O_h $[\text{Tl}_6]^{6-}$ clusters can also afford a pseudogap at E_F . So the hypothetical KTI does not require 2 more electrons per (K_6Tl_6) unit to achieve a closed-shell configuration—it is already (almost) closed-shell. Therefore, even without JT distortion, SOC alleviates the “hypo-electronicity” with respect to Wade–Mingos rules. This means that a different electron counting scheme is required to rationalize the clusters formed by heavy elements featuring significant relativistic SOC effects.

In real KTI (Figure 6b), JT and SOC cooperatively effect an enhanced band gap opening ($\sim 0.19 \text{ eV}$) at E_F . Finally, we can achieve a quantitative evaluation of the impact of JT and SOC by comparing the respective total energy values of the real and hypothetical KTI. When SOC is ignored, real KTI is lower in energy than the hypothetical by 0.21 eV per (K_6Tl_6) unit, indicating that the JT effect favors the structure with “compressed” $[\text{Tl}_6]^{6-}$. When SOC is considered, although the real KTI is still energetically favorable, its energy advantage over the hypothetical KTI drops to only 0.09 eV per (K_6Tl_6) unit. So, apparently, SOC substantially stabilizes the structure with undistorted O_h $[\text{Tl}_6]^{6-}$, making it energetically more competitive.

Excised Clusters $[\text{A}_8\text{Tl}_6]^{2+}$ and A_8Tl_6 . As mentioned above, treating the $[\text{Tl}_6]^{6-}$ cluster as an isolated polyanion is

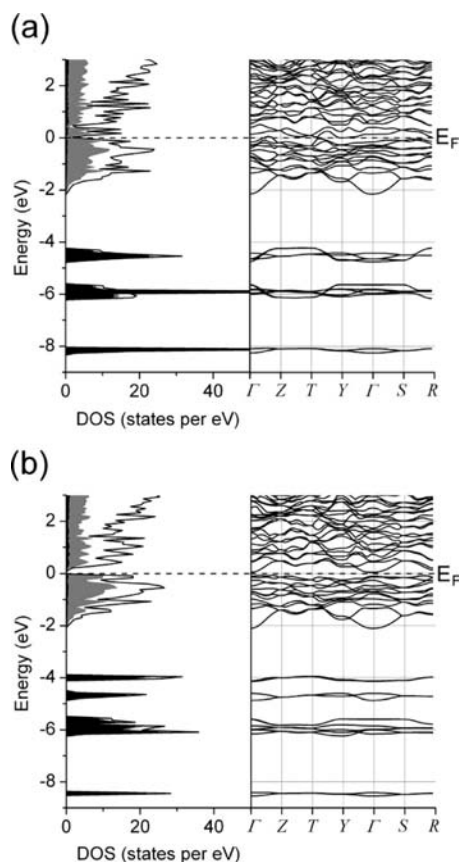


Figure 6. The SOC DOS curves and band structures of (a) hypothetical KTI with O_h $[\text{Tl}_6]^{6-}$ and (b) real KTI with C_{2h} $[\text{Tl}_6]^{6-}$ (black: Tl s; gray: Tl p; white: K).

not stringent but a plausible approximation. Most of the previous works are based on calculations assuming high formal charges, which causes no problem on the extended Hückel level of theory. For our first-principle DFT calculations, however, the highest orbitals of such negatively charged clusters would be unbound due to the Coulomb repulsion of the electrons. So, as demonstrated previously on $\text{Cs}_{18}\text{Tl}_8\text{O}_6$,²⁰ we have to compensate the charges by adding alkali metal cations. For instance, we use $[\text{Cs}_8\text{Tl}_6]^{2+}$ as a model for the $[\text{Tl}_6]^{6-}$ cluster (upper graphs in Figure 7) and Cs_8Tl_6 models the Wade analogue $[\text{Tl}_6]^{8-}$ (lower graphs in Figure 7). The alkali metal cations cap the eight faces of the octahedron.

We have demonstrated the superimposing stabilization caused by JT and SOC in the previous chapter with band structure calculations. By focusing on the charge compensated excised clusters, we can provide a more sophisticated and comprehensive demonstration by monitoring the total energy of the excised $[\text{Cs}_8\text{Tl}_6]^{2+}$ and Cs_8Tl_6 clusters as a function of the distortion of the octahedron. These results are shown as one-dimensional cross sections of energy landscapes (see Figure 7). For each point on the line, the ratio of the edge lengths $R(\text{basal})/R(\text{apical})$ was fixed and all other structural parameters were optimized, while constrained to D_{4h} symmetry.

For the scalar relativistic calculations (non-SOC) within the unrestricted open-shell Kohn–Sham formalism (UKS), the spin-state is fixed for each energy landscape. On the left column of Figure 7 we show the lowest lying singlet and triplet curves. In contrast, the spin and orbital moments are coupled in the two-component calculations (SOC, Figure 7 right column) and

the (fractional) number of unpaired electrons N_S (eq 2) may vary along a scan line. All the minima of the ΔE curves in Figure 7, with one exception, the upper left minimum in the SOC curve of Cs_8Tl_6 with $R(\text{basal})/R(\text{apical}) < 1$ (lower right graph in Figure 7), are real local minima on the energy landscapes, as the respective Hessian matrices have no negative eigenvalues.

The inspection of the ΔE diagrams reveals clearly qualitative and quantitative differences between the non-SOC and the SOC cases. The lowest non-SOC minimum is a singlet state with a fully occupied e_u -HOMO and an a_{2u} -LUMO, representing a compressed polyhedron. When the edge length ratio $R(\text{basal})/R(\text{apical})$ approaches, and goes beyond, unity, a triplet state, although substantially higher in energy, becomes more favorable (HOMO, half filled e_u ; LUMO, e_u). With inclusion of SOC (Figure 7 upper right graph), the cluster is a closed-shell system all along the scan. Moreover a second minimum appears at an edge ratio of 1.0, corresponding to a regular octahedron. The energy difference of both minima of the energy landscape is as small as 4.5 kJ/mol. Thus both minima become competitive and both configurations have actually been observed experimentally.¹⁹

With the Wade analogue $[\text{Tl}_6]^{8-}$ in Cs_8Tl_6 , both, the singlet (HOMO, a_{2u} ; LUMO, e_u) and the triplet (HOMO, half-filled e_u ; LUMO, a_{2u}) correspond to a compressed octahedron in the scalar relativistic approximation. The singlet is more favorable at lower edge ratios (Figure 7 lower left). Again, there is a significant change in the characteristics of the energy landscape, if SOC is considered. The ΔE curve is more flat and the cluster becomes an open-shell system ($N_S < 1.66$) with lower edge ratios. As demonstrated here on the example of excised charge-compensated Tl_6^{6-} cluster anions, performing a full relativistic treatment has enabled us to reconcile apparently contradictory experimental observation of distorted and undistorted clusters in spite of identical numbers of skeletal electrons.

Besides assessing the total energies involved, these studies into excised clusters can also provide us with a deeper understanding of how JT and SOC affect electronic structures and electron configurations. Figure 8 displays the non-SOC molecular orbital (MO) diagram of a $[\text{K}_8\text{Tl}_6]^{2+}$, whose structure was optimized with its symmetry restrained to C_{2h} , mimicking the $[\text{Tl}_6]^{6-}$ clusters in KTI. The resulting $[\text{K}_8\text{Tl}_6]^{2+}$ has, however, a symmetry of D_{4h} . The lowest 6 MOs from $1a_{1g}$ to $2a_{1g}$ are mainly composed of spherical Tl 6s orbitals. The splitting of these levels on the energy scale arises from the nodal structure of the canonical orbitals. A localization procedure leads to degenerate local orbitals at the single thallium sites (basal, -13.14 eV; apical, -13.09 eV) consisting predominantly of the s functions at the respective site. This reveals the “inert” pair characteristics of Tl 6s electrons, and is in agreement with the band structure calculations.

The MOs from $1e_g$ to $2e_u$ are cluster-bonding MOs, and they bear evident resemblance in topology with the charge density maps of the KTI bands shown in Figure 4. Also like KTI, the D_{4h} $[\text{K}_8\text{Tl}_6]^{2+}$ has closed-shell electron configuration with a HOMO–LUMO gap of 1.43 eV. All of these consistencies between KTI band structure and $[\text{K}_8\text{Tl}_6]^{2+}$ MO diagram prove that the excised cluster can really serve as good approximation for the complete solid.

We also optimized the structure of $[\text{K}_8\text{Tl}_6]^{2+}$ by restricting the symmetry to O_h . When SOC is ignored, it has an open-shell electron configuration (Figure 9, O_h non-SOC). Each of the three degenerate $2t_{1u}$ HOMOs has an average occupancy of 4/

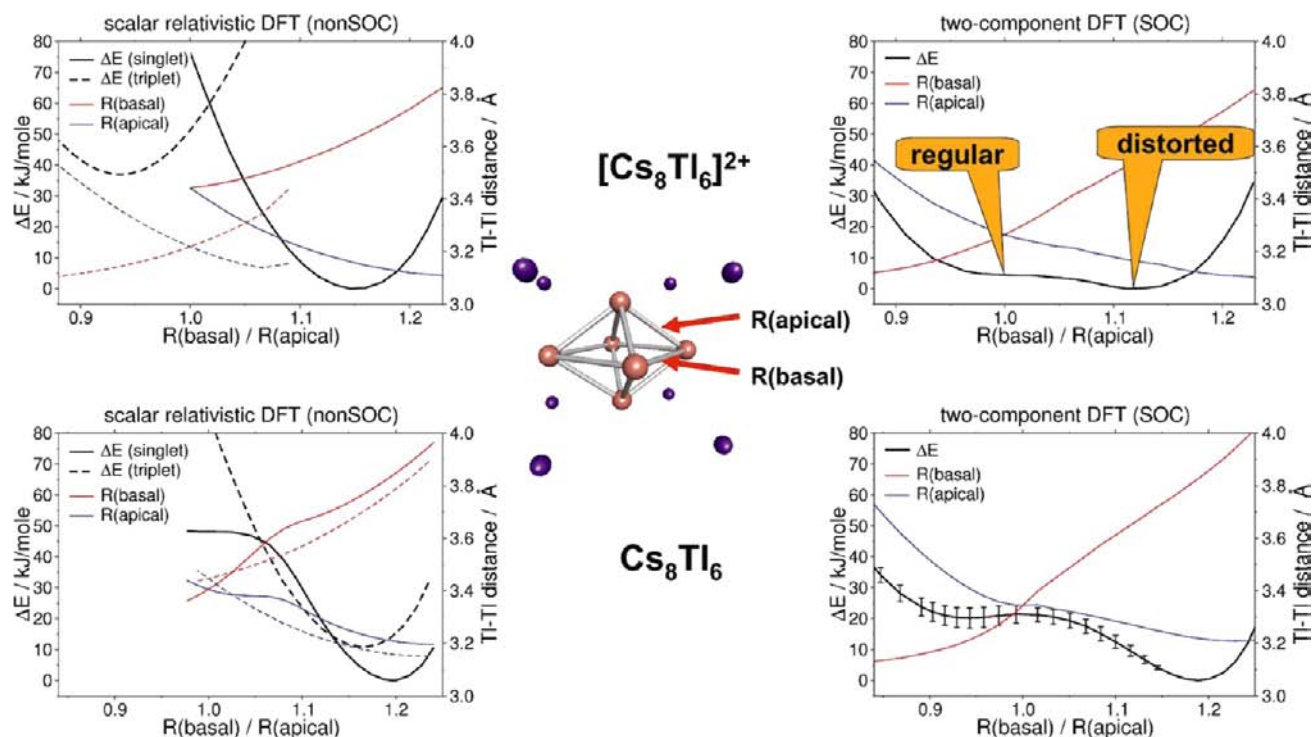


Figure 7. One-dimensional scan through the energy landscapes of $[\text{Cs}_8\text{Ti}_6]^{2+}$ (upper graphs) and Cs_8Ti_6 (lower graphs). The left ordinate represents the energy relative to the minimum of the scan line (ΔE), the right one the Ti–Ti distances. The left graphs show the results of scalar relativistic DFT calculations (unrestricted KS singlet and triplet), and the right ones are based on two-component DFT including SOC. In addition, the lower right graph shows bars representing the number of unpaired electrons N_s (eq 2) (<1.66).

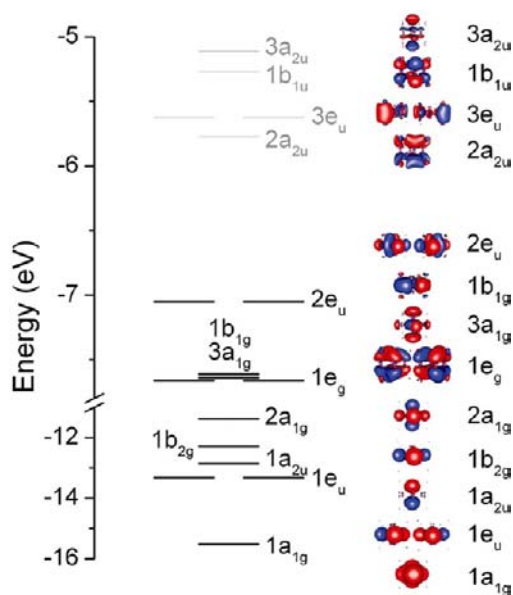


Figure 8. Molecular orbital energy levels of D_{4h} $[\text{K}_8\text{Ti}_6]^{2+}$ and their isosurface sketches (black, occupied; gray, empty).

3. With two more electrons, it would achieve a closed-shell configuration and satisfy Wade–Mingos rules. This is consistent with the electron deficiency shown above in the non-SOC band structure of the hypothetical KTI with O_h $[\text{Ti}_6]^{6-}$ clusters (Figure 5).

The band structure calculations have revealed that JT and SOC can both open a band gap at E_F , thus affording a closed-shell electronic configuration for KTI. The mechanism of this band gap opening can be illustrated by comparing the non-

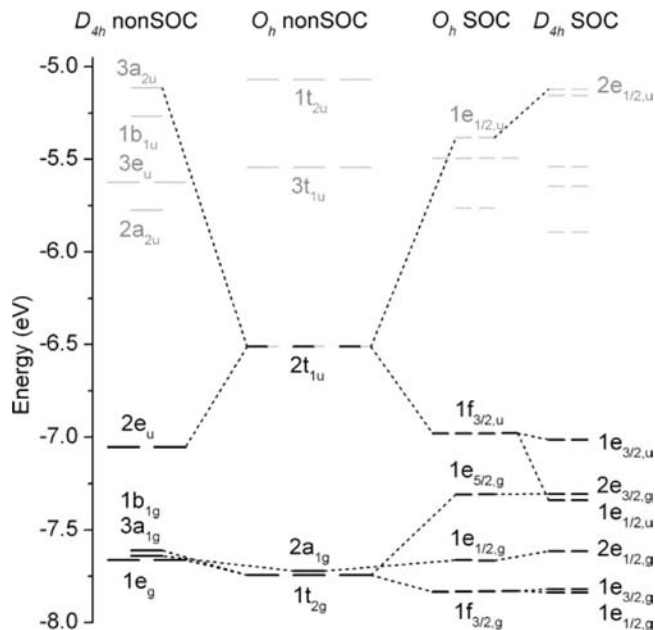


Figure 9. Molecular orbitals (non-SOC) and spinors (SOC) of O_h and D_{4h} $[\text{K}_8\text{Ti}_6]^{2+}$ (black, occupied; gray, empty).

SOC MO diagrams and the SOC spinor diagrams of the D_{4h} $[\text{K}_8\text{Ti}_6]^{2+}$ and the O_h $[\text{K}_8\text{Ti}_6]^{2+}$ in Figure 9. It shows that JT and SOC can both break the degeneracy of the partially populated $2t_{1u}$ shell and lead to a closed-shell configuration and a large HOMO–LUMO gap. JT effect reduces the symmetry of $[\text{K}_8\text{Ti}_6]^{2+}$ from O_h to D_{4h} , the irrep T_{1u} of O_h decomposes into $E_u \oplus A_{2u}$ in D_{4h} . So the $2t_{1u}$ shell splits into fully occupied $2e_u$ and empty $3a_{2u}$ shells. SOC has a similar effect. As mentioned

above, T_{1u} of point group O_h is subduced into two spinor irreps in the double group O_h^* , $F_{3/2,u} \oplus E_{1/2,u}$. So when SOC is considered, the $2t_{1u}$ HOMO shell splits into fully occupied $1f_{3/2,u}$ and empty $1e_{1/2,u}$. (The correspondence between orbitals and spinors are established by examining their isosurface maps, details are given in Supporting Information.) Furthermore, when SOC and JT are both evaluated, the $1f_{2/3,u}$ shell further split into the $1e_{1/2,u}$ and $1e_{3/2,u}$ shells in D_{4h} SOC, with both of them occupied and the former lowering significantly in its energy. This energy lowering occurs at the expense of the energy rise from the empty $1e_{1/2,u}$ shell in O_h SOC to the $2e_{1/2,u}$ shell in D_{4h} SOC. So with SOC, the O_h -to- D_{4h} distortion corresponds to a second-order JT effect.

In conclusion, as demonstrated with both crystals and excised clusters, JT and SOC energetically stabilize the formal $[Tl_6]^{6-}$ by opening a gap. For the compounds whose $[Tl_6]^{6-}$ clusters have $\sim O_h$ symmetry, such as Cs_4Tl_2O and the hypothetical KTI, SOC is the only stabilization mechanism. For those compounds with geometrically “compressed” $[Tl_6]^{6-}$ clusters, such as KTI, $CsTl$, and $A_{10}Tl_6O_2$ (A = alkali metal), the stabilization is due to the cooperative effects of SOC and second order JT.

The reconciliation of electron deficiency by JT and SOC is not unique to the compounds with formal $[Tl_6]^{6-}$ clusters, but can also be applied to all the other “hypo-electronic” Tl cluster compounds with closed-shell electronic configurations listed in Figure 1. We have successfully rationalized the isomeric $[Tl_8]^{6-}$ clusters in $Cs_{18}Tl_8O_6$ and Cs_8Tl_8O in our previous report with similar arguments.²⁰ Besides, $Na_2K_{21}Tl_{19}$ is also electron exact although it has the “hypo-electronic” formal $[Tl_9]^{9-}$ clusters.¹³ This can be rationalized as the result of a JT distortion starting from the Wade–Mingos *closo* geometry, a tricapped trigonal prism. Details are in the Supporting Information.

CONCLUSIONS

We present the results of calculations and analyses to resolve the enigma of thallium cluster anions. For the vast majority of inorganic cluster compounds, there exist qualitative concepts, with which one can reconcile the number of valence electrons in a cluster with its topology and stability. Such approaches as the Zintl–Klemm concept or Wade–Mingos’s rules may fail, however, when applied to thallium cluster anions. Since all the thallium clusters defying the heuristic systematics have in common less skeleton electrons than the required by the rules mentioned, they were classified as “hypo-electronic”. This term, however, is just a designation and does not provide any explanation.

While including all homoatomic and noncentered thallium clusters, we give particular emphasis to the cases of $[Tl_6]^{6-}$ and $[Tl_8]^{6-}$ clusters, featuring most intricate ramifications. Intriguingly, for the same number of cluster atoms and the same electron counts, different geometries were encountered experimentally. At the same time, clusters of both respective geometries experienced electronic stabilization as indicated by HOMO–LUMO gaps opening. $[Tl_6]^{6-}$ exists as an ideal ($\sim O_h$) and compressed ($\sim D_{4h}$) octahedron in different compounds featuring closed-shell electron configurations. For $[Tl_8]^{6-}$, the most regular structure possible, a cube, is not realized. Instead, two substantially different distortion variants, the “tetrahedral star” and “parallelepiped” topologies, were found experimentally.

Our band structure calculations on the complete experimental extended structures as well as electronic structure calculations on geometry optimized and charge compensated

excised clusters on two different levels of theory, scalar relativistic and full relativistic including SOC, have revealed that the thallium compounds investigated experience electronic stabilization by JT distortion and relativistic SOC, independently, or concomitantly in a synergic fashion.

Cs_4Tl_2O , for instance, contains a regular octahedral cluster $[Tl_6]^{6-}$ as constitutional component and has been shown to be diamagnetic. Such a cluster would require two more electrons in order to fulfill Wade’s rules, and thus was addressed as “hypo-electronic”. However, a full relativistic treatment has revealed that considering SOC opens a gap, thus lifting the degeneracy of the partly filled HOMO (in a scalar relativistic analysis). In experimental KTI, a band gap opens due to a symmetry reduction of the $[Tl_6]^{6-}$ cluster from O_h to D_{4h} . Here, the electronic stabilization is further enhanced by SOC. Similarly, as reported in our previous work,²⁰ for D_{3d} $[Tl_8]^{6-}$ in Cs_8Tl_8O , the JT effect is sufficient to open a gap, while the existence of the tetrahedral star configuration (T_d) of $[Tl_8]^{6-}$ in $Cs_{18}Tl_8O_6$ can only be understood if fully relativistic theory is applied.

The two major factors of influence, JT distortion and SOC, thus generate energy landscapes of thallium cluster compounds, which feature for species with identical number of atoms per cluster and identical overall charges different local minima, corresponding to different structures. With respect to total energies, there is still a hierarchical order; e.g., T_d $[Tl_8]^{6-}$ is more stable than the D_{3d} variant. Which one of these intrinsically stable clusters topologies are realized in a specific extended solid is subject to the minimization of the total energy of the latter.²⁰

As a quintessence, we conclude that the term “hypo-electronic” is not appropriate to describe thallium cluster anions. On the contrary, the clusters encountered thus far appear to be electronically saturated. This view is also receiving support from the experimental conditions at which such compounds are synthesized, namely, applying an excess of the respective alkali metal, which, due to its extremely low work function, provides abundant electrons.

Finally, our findings allow us to qualitatively analyze heavy atoms’ clusters on an improved level of understanding. The recipe to be followed can be extracted from Figure 9. One performs two independent group theoretical analyses, starting from an aristotypical topology (of the highest symmetry possible). In one procedure, reductions in point group symmetry are identified that are suited to lift the degeneracy (of partly filled frontier orbitals) and to open a gap (JT effect). Second, applying the double group approach, the splittings of the electronic states caused by SOC are analyzed, while keeping the symmetry unchanged. Finally, a superposition of both effects, if applicable, yields the combined impact. In this way, it is possible to rationalize which distortion and which SOC-induced splittings of the electronic states involved are suited to generate a closed-shell electronic configuration for a cluster of given atom and electron count.

ASSOCIATED CONTENT

Supporting Information

Details of the hypothetical KTI model structure; pictorial demonstration of the correspondence between orbitals/spinors; discussion of $Na_2K_{21}Tl_{19}$; and the details of WIEN2k calculations. This material is available free of charge via the Internet at <http://pubs.acs.org>.

■ AUTHOR INFORMATION

Corresponding Author

m.jansen@fkf.mpg.de

Notes

The authors declare no competing financial interest.

■ REFERENCES

- (1) Jansen, M. *Angew. Chem., Int. Ed.* **2002**, *41*, 3747–3766.
- (2) Hoffmann, R. J. *Mol. Struct.: Theochem.* **1998**, *424*, 1–6.
- (3) Jansen, M.; Wedig, U. *Angew. Chem., Int. Ed.* **2008**, *47*, 10026–10029.
- (4) Zintl, E.; Dullenkopf, W. *Z. Phys. Chem.* **1932**, *B16*, 195–205. Zintl, E.; Neumayr, S. *Z. Phys. Chem.* **1933**, *B20*, 272–275. Zintl, E.; Woltersdorf, G. *Z. Elektrochem.* **1935**, *41*, 876–879. Zintl, E. *Angew. Chem.* **1939**, *52*, 1–100. Klemm, W. *Proc. Chem. Soc. London* **1958**, 329.
- (5) Schäfer, H.; Eisenman, B.; Müller, W. *Angew. Chem., Int. Ed.* **1973**, *12*, 694–712. Schäfer, H. *Annu. Rev. Mater. Sci.* **1985**, *15*, 1–42.
- (6) *Chemistry, Structure, and Bonding of Zintl Phases and Ions*; Kauzlarich, S. M., Ed.; VCH: Weinheim, Germany, 1996.
- (7) Wade, K. J. *Chem. Soc. D, Chem. Commun.* **1971**, *15*, 792–793. Wade, K. *Inorg. Nucl. Chem. Lett.* **1972**, *8*, 559–562. Wade, K. *Inorg. Nucl. Chem. Lett.* **1972**, *8*, 823–827. Housecroft, C. E.; Wade, K. *Gazz. Chim. Ital.* **1980**, *110*, 87–95.
- (8) Mingos, D. M. P. *Nature Phys. Sci.* **1972**, *236*, 99–102. Mingos, D. M. P. *Acc. Chem. Res.* **1984**, *17*, 311–319. Mingos, D. M. P. *Pure Appl. Chem.* **1991**, *63*, 807–812.
- (9) King, R. B.; Rouvray, D. H. *J. Am. Chem. Soc.* **1977**, *99*, 7834–7840.
- (10) Wang, F.; Miller, G. J. *Inorg. Chem.* **2011**, *50*, 7625–7636.
- (11) Corbett, J. D. *Angew. Chem., Int. Ed.* **2000**, *39*, 670–690.
- (12) Pyykkö, P.; Desclaux, J.-P. *Acc. Chem. Res.* **1979**, *12*, 276–281.
- (13) Dong, Z. C.; Corbett, J. D. *J. Am. Chem. Soc.* **1994**, *116*, 3429–3435.
- (14) Dong, Z. C.; Corbett, J. D. *J. Am. Chem. Soc.* **1993**, *115*, 11299–11303.
- (15) Dong, Z. C.; Corbett, J. D. *Inorg. Chem.* **1996**, *35*, 2301–2306.
- (16) Karpov, A.; Jansen, M. *Chem. Commun.* **2006**, 1706–1708.
- (17) Kaskel, S.; Corbett, J. D. *Inorg. Chem.* **2000**, *39*, 778–782.
- (18) Huang, D. P.; Dong, Z. C.; Corbett, J. D. *Inorg. Chem.* **1998**, *37*, 5881–5886.
- (19) Saltykov, V.; Nuss, J.; Wedig, U.; Jansen, M. *Z. Anorg. Allg. Chem.* **2011**, *637*, 357–361.
- (20) Wedig, U.; Saltykov, V.; Nuss, J.; Jansen, M. *J. Am. Chem. Soc.* **2010**, *132*, 12458–12463.
- (21) Pitzer, K. S. *Acc. Chem. Res.* **1979**, *12*, 271–276.
- (22) *Relativistic Electronic Structure Theory*; Schwerdtfeger, P., Ed.; Elsevier Science: Amsterdam, The Netherlands, 2002.
- (23) Sevov, S. C.; Corbett, J. D. *Z. Anorg. Allg. Chem.* **1993**, *619*, 128–132.
- (24) Saltykov, V.; Nuss, J.; Wedig, U.; Prasad, D. L. V. K.; Jansen, M. *Z. Anorg. Allg. Chem.* **2011**, *637*, 834–839.
- (25) Karpov, A.; Jansen, M. *Angew. Chem., Int. Ed.* **2005**, *44*, 7639–7643.
- (26) Hansen, D. A.; Smith, J. F. *Acta Crystallogr.* **1967**, *22*, 836–845.
- (27) Dong, Z. C.; Corbett, J. D. *Inorg. Chem.* **1996**, *35*, 3107–3112.
- (28) Dong, Z. C.; Corbett, J. D. *Angew. Chem. Int. Ed.* **1996**, *35*, 1006–1009.
- (29) Dong, Z. C.; Corbett, J. D. *J. Cluster Sci.* **1995**, *6*, 187–201.
- (30) Dong, Z. C.; Corbett, J. D. *Inorg. Chem.* **1996**, *35*, 1444–1450.
- (31) Saltykov, V. *The Relativistic Effect in Intermetallic Phases of Gold, Platinum, and Thallium*. Ph.D. Thesis, Max Planck Institute for Solid State Research, Stuttgart, Germany, 2011.
- (32) Perdew, J. P.; Burke, K.; Ernzerhof, M. *Phys. Rev. Lett.* **1996**, *77*, 3865.
- (33) Blaha, P.; Schwarz, K.; Madsen, G. K. H.; Kvasnicka, D.; Luitz, J. *WIEN2k, An Augmented Plane Waves + Local Orbitals Program for Calculating Crystal Properties*; Schwarz, K., Ed.; Techn. Universität Wien: Austria, 2001; ISBN 3-9501031-1-2.
- (34) Kresse, G.; Furthmüller, J. *Phys. Rev. B* **1996**, *54*, 11169.
- (35) Sjöstedt, E.; Nordström, L.; Singh, D. J. *Solid State Commun.* **2000**, *114*, 15.
- (36) Madsen, G. K. H.; Blaha, P.; Schwarz, K.; Sjöstedt, E.; Nordström, L. *Phys. Rev. B* **2001**, *64*, 195134.
- (37) Blöchl, P. E. *Phys. Rev. B* **1994**, *50*, 17953.
- (38) Kresse, G.; Joubert, D. *Phys. Rev. B* **1999**, *59*, 1758.
- (39) Koelling, D. D.; Harmon, B. N. J. *Phys. C.: Solid State Phys* **1977**, *10*, 3107.
- (40) Novák, P. http://www.wien2k.at/reg_user/textbooks/novak_lecture_on_spinorbit.ps.
- (41) Hobbs, D.; Kresse, G.; Hafner, J. *Phys. Rev. B* **2000**, *62*, 11556–11570.
- (42) *TURBOMOLE, V6.3*; University of Karlsruhe and Forschungszentrum Karlsruhe GmbH, TURBOMOLE GmbH, 2011, <http://www.turbomole.com>.
- (43) v. Arnim, M.; Ahlrichs, R. *J. Comput. Chem.* **1998**, *19*, 1746.
- (44) Metz, B.; Schweizer, M.; Stoll, H.; Dolg, M.; Liu, W. *Theor. Chem. Acc.* **2000**, *104*, 22–28.
- (45) Leininger, T.; Nicklass, A.; Küchle, W.; Stoll, H.; Dolg, M.; Bergner, A. *Chem. Phys. Lett.* **1996**, *255*, 274–280.
- (46) Weigend, F.; Ahlrichs, R. *Phys. Chem. Chem. Phys.* **2005**, *7*, 3297–3305.
- (47) Armbruster, M. K.; Weigend, F.; van Wüllen, C.; Klopper, W. *Phys. Chem. Chem. Phys.* **2008**, *10*, 1748–1756.
- (48) Weigend, F.; Baldes, A. *J. Chem. Phys.* **2010**, *133*, 174102.
- (49) Otero-de-la-Roza, A.; Blanco, M. A.; Martín Pendás, A.; Luaña, V. *Comput. Phys. Commun.* **2009**, *180*, 157–166.
- (50) Kokalj, A. *Comput. Mater. Sci.* **2003**, *28*, 155–168.
- (51) Momma, K.; Izumi, F. *J. Appl. Crystallogr.* **2011**, *44*, 1272–1276.
- (52) Dirac, P. A. M. *Proc. Royal Soc. London, Ser. A* **1928**, *117*, 610.
- (53) Chisholm, C. D. H. *Group Theoretical Techniques in Quantum Chemistry*. Academic Press: London, 1976.
- (54) Böhm, M. *Symmetrien in Festkörpern: Gruppentheoretische Grundlagen und Anwendungen*. Wiley-VCH: Berlin, 2002.
- (55) Altmann, S. L.; Herzig, P., *Point-group theory tables*; Clarendon Press/Oxford University Press: Oxford/New York, 1994.
- (56) David, J.; Fuentealba, P.; Restrepo, A. *Chem. Phys. Lett.* **2008**, *457*, 42–44. David, J.; Guerra, D.; Restrepo, A. *Inorg. Chem.* **2011**, *50*, 1480–1483.
- (57) Poluyanov, L. V.; Domcke, W. *J. Chem. Phys.* **2012**, *137*, 114101.
- (58) Edwards, P. A.; Corbett, J. D. *Inorg. Chem.* **1977**, *16*, 903.
- (59) Corbett, J. D. *Inorg. Chem.* **1968**, *7*, 198.
- (60) Krebs, B.; Mummert, M.; Brendel, C. *J. Less-Common Met.* **1986**, *116*, 159.
- (61) Baldes, A.; Gulde, R.; Weigend, F. *J. Clust. Sci.* **2011**, *22*, 355.
- (62) Bader, R. F. W. *Atoms in Molecules: A Quantum Theory*; Oxford University Press: Oxford, 1990.